Light-Tunable Charge Density Wave Orders in $MoTe_2$ and WTe_2 Single Layers

Giovanni Marini[1,*] and Matteo Calandra[2,1,3,†]
[1]Graphene Labs, Fondazione Istituto Italiano di Tecnologia, Via Morego, I-16163 Genova, Italy
[2]Department of Physics, University of Trento, Via Sommarive 14, 38123 Povo, Italy
[3]Sorbonne Université, CNRS, Institut des Nanosciences de Paris, UMR7588, F-75252, Paris, France

(Received 2 June 2021; accepted 18 November 2021; published 17 December 2021)

By using constrained density functional theory modeling, we demonstrate that ultrafast optical pumping unveils hidden charge orders in group VI monolayer transition metal ditellurides. We show that irradiation of the insulating $2H$ phases stabilizes multiple transient charge density wave orders with light-tunable distortion, periodicity, electronic structure, and band gap. Moreover, optical pumping of the semimetallic $1T'$ phases generates a transient charge ordered metallic phase composed of 2D diamond clusters. For each transient phase we identify the critical fluence at which it is observed and the specific optical and Raman fingerprints to directly compare with future ultrafast pump-probe experiments. Our work demonstrates that it is possible to stabilize charge density waves even in insulating 2D transition metal dichalcogenides by ultrafast irradiation.

DOI: 10.1103/PhysRevLett.127.257401

Designing and manipulating broken symmetry states with laser light is an appealing perspective as it can lead to the discovery of hidden ordered states and enable control over a broad range of material properties [1,2]. Few-layer transition metal dichalcogenides (TMDs) are an ideal class of materials for ultrafast investigations, mainly for two reasons. First, metallic dichalcogenides display the occurrence of competing orders such as charge density wave (CDW) phases and superconductivity. Second, insulating TMDs normally do not display charge ordering but have typical gaps in the 1–2.5 eV range [3], ideal for optical pumping. Inducing a CDW in insulating dichalcogenides is important as it could lead to new low-dimensional phases with unexpected topological and correlation properties.

Particularly relevant are $MoTe_2$ and WTe_2 as the barrier existing between the $2H$ and the $1T'$ phase is lower compared to the other compounds of the family [4]. The most stable $MoTe_2$ polytype is the $2H$ phase, however, it has been shown that a transition towards the $1T'$ can be selectively activated in ultrathin layers by means of electrostatic doping [5], tensile strain [6], and laser irradiation [7]. Conversely, WTe_2 is stable in the $1T'$ polytype and the metastable $2H$ phase has been synthesized only recently [8,9].

Most of the work carried out on irradiated $MoTe_2$ concerns the irreversible $2H$-$1T'$ phase transition. However, irreversible phase transitions are only a small part of the broken symmetry charge ordered states available after laser irradiation, as reversible transition towards transient phases can occur; these can be detected either by ultrafast x-ray diffraction at x-ray free electron laser facilities [10] or by pump-probe experiments to measure optical or Raman spectra after the electronic excitation [11,12].

Phase transitions under ultrafast irradiation have been observed for conventional semiconductors under intense ultrafast irradiation [13,14] (nonthermal melting), in phase-change materials [10], and have been proposed to occur in ferroelectrics [15]. However, in most of these cases, the ordered phase is present in the ground state and suppressed by irradiation. Very few detections of hidden CDW orders (i.e., the ordered phase is a transient state induced by light) have been devised or demonstrated [16]. Furthermore, it is unclear if hidden orders are present in single layer dichalcogenides and at what fluence they can be observed.

In this work we demonstrate the occurrence of multiple charge ordered transient states in $MoTe_2$ and WTe_2 single layers after ultrafast irradiation of the $2H$ and $1T'$ phases in the high-excitation density regime [$n_e \geq 10^{14}\ e^-/\mathrm{cm}^2$, where n_e represents the photocarrier concentration (PC)]. Moreover we show the occurrence of a light-induced band gap closing in the $2H$ phases. Finally, we identify specific spectroscopic fingerprints of each phase that will allow its detection in future ultrafast experiments. We investigate the effect of laser irradiation within density functional theory (DFT). In the case of insulators, we suitably constrain the occupations of the Kohn-Sham conduction eigenstates in order to mimic the thermalized photocarrier population. This approach has been described in Ref. [17] and we refer to it as constrained DFT (CDFT). We implemented the CDFT technique as well as the calculation of forces and stress tensor in the presence of an electron-hole plasma within the QUANTUM ESPRESSO distribution [18,19]. In the case of metals and semimetals ($1T'$ phases), the radiative electron-hole recombination is fast [20,21], thus laser excitation is simulated employing Fermi-Dirac occupations

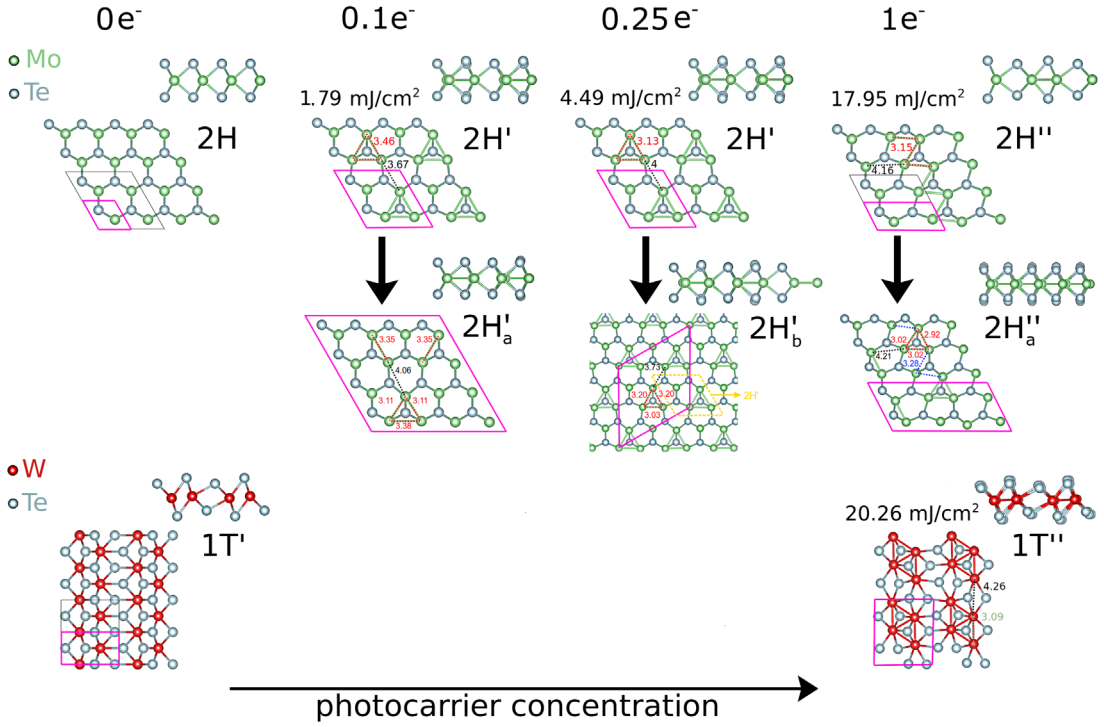

FIG. 1. Schematic representation of hidden orders in monolayer dichalcogenides. Upper panel: $2H$-$MoTe_2$ as a function of the PC (f.u.). Mo clusterization is represented by green bonds. At $n_e = 0.25\ e^-/\text{f.u.}$ ($n_e = 1\ e^-/\text{f.u.}$) the energy gain associated to the $2H \to 2H'$ ($2H \to 2H''$) distortion is 107.2 (583.1) meV/f.u., while the $2H' \to 2H'_b$ ($2H'' \to 2H''_a$) distortion has an energy gain of only 3.1 (6.6) meV/f.u. Lower panel: $1T'$-WTe_2 as a function of the PC (f.u.). Numbers in the crystal structure images represent atomic distances in Å. For the relation between fluence and PC see the SM.

at high temperature. All the simulation details are reported in the Supplemental Material (SM) [22], which includes Refs. [23–53].

The main results of our Letter are summarized in Figs. 1 and 2. First, we find that light induces a progressive formation of CDW order in $2H$-$MoTe_2$ (and $2H$-WTe_2), starting already at $n_e = 0.1\ e^-$ per formula unit (f.u.). The hidden CDW order, labeled $2H'$, arises from an imaginary phonon frequency in correspondence to the **M** point of the Brillouin zone (BZ) and involves clustering of three Mo atoms [the soft phonon pattern involves the displacement of Mo atoms only, see Fig. 2(b)]. The $2H'$ phase is in turn prone to structural instabilities, in particular two lower symmetry phases compete; we refer to them as $2H'_a$ and $2H'_b$. Most importantly, the $2H'$ phase, and the derived a and b distorted structures, display a progressive band gap closing with increasing PC and transition to a metallic state at $n_e = 0.25\ e^-/\text{f.u.}$ [see Figs. 2(d) and 2(e)]. At $n_e = 1\ e^-/\text{f.u.}$ (still reachable by current laser sources) a new 2×1 CDW appears, composed of alternating anisotropically compressed and expanded stripes of hexagons. We label this phase $2H''$. The $2H''$ phase is in turn unstable and relaxes towards a lower symmetry structure, named $2H''_a$ phase.

Second, pumping on top of the $1T'$-$MoTe_2$ and $1T'$-WTe_2 phases at $n_e \approx 1\ e^-/\text{f.u.}$ stabilizes a 2×2 hidden CDW order composed of 2D diamond clusters of transition metal atoms (see Fig. 1 bottom right), that we label $1T''$. In the absence of optical pumping, this CDW structure has been found as metastable and competing with the $1T'$ phase in MoS_2 [54], and has been occasionally detected in some MoS_2 single layers [55]. Thus, laser light can be used to reveal hidden charge density wave orders, hard to stabilize in standard thermochemical conditions. Finally, we note that energy transfer from the electrons to the lattice could reduce the effective temperature to be considered in the simulations, suggesting that the critical PC for the stabilization of the $1T''$ phase is somewhat underestimated.

We now study the mechanism destabilizing the $2H$ structures in detail (for the analysis of the CDW formation in $1T'$ phases see the SM). We consider $MoTe_2$, but similar results for WTe_2 are shown in the SM. We perform supercell finite difference calculations of the phonon frequencies at specific high-symmetry points. The results are plotted in Figs. 2(a), 2(b), and 2(c). Raman active phonons at Γ are plotted in red. At low PCs, in a single-valley direct gap semiconductor, momentum and energy conservation enforce that only zone center phonons can be excited. Typically, if free internal coordinates are present, this results in displacive excitation of coherent Raman phonons. $MoTe_2$ is a two-valley semiconductor and

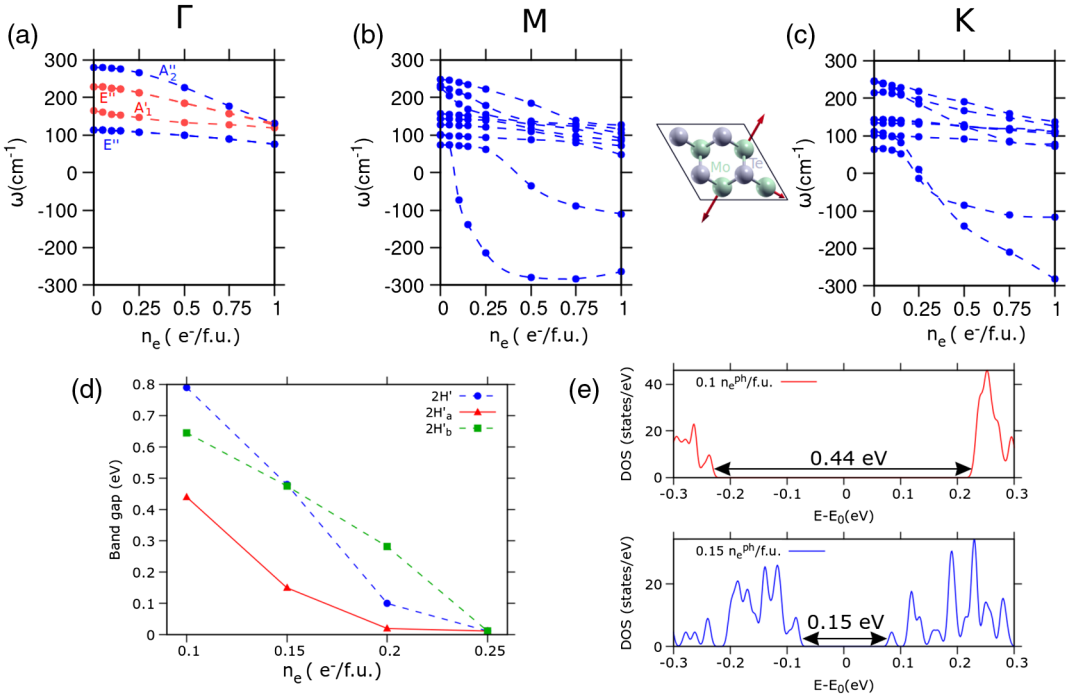

FIG. 2. (a),(b),(c) Phonon frequencies as a function of PC for $2H$-$MoTe_2$ at $\mathbf{\Gamma}$, $\mathbf{M}$, $\mathbf{K}$ points of the BZ, respectively. Raman active modes at $\mathbf{\Gamma}$ are depicted in red. The lowest eigenvector at the $\mathbf{M}$ point is schematically depicted in panel (b). (d) Electronic band gap as a function of PC. (e) Density of states for the $2H'_a$ phase of $MoTe_2$ at $n_e = 0.1$ and 0.15 e^-/f.u.

phonon excitations at $\mathbf{\Gamma}$ and $\mathbf{K}$ are both possible. As it can be seen in Fig. 2(a) the A'_1 mode softens under weak photoexcitation. Recently it was suggested that phonon softenings at $\mathbf{\Gamma}$ drive the irreversible $2H$-$1T'$ transition in monolayer $MoTe_2$ [56]. However, we find that even at large PCs $\mathbf{\Gamma}$ frequencies never become imaginary [Fig. 2(a)], invalidating this claim. We find that a critical PC of $n_e \approx 1.75$ e^-/f.u., corresponding to a high fluence of 31.41 mJ/cm^2, is needed to destabilize $\mathbf{\Gamma}$ phonons, suggesting that other concomitant mechanisms such as Te vacancy creation are involved in the irreversible $2H \rightarrow 1T'$ transition [57]. At higher PCs instabilities can also occur at other phonon momenta. Already at $n_e = 0.1$ e^-/f.u., $\mathbf{M}$-point phonons are strongly imaginary. In order to understand the mechanism responsible for the formation of the $2H'$ phases and to decouple the role of conduction and valence states in the CDW formation, we also calculate the phonon frequency spectrum within a rigid doping approximation, simulating an electron charge excess or deficiency. The rigid doping calculations show that both conduction and valence states contribute to the $\mathbf{M}$-point phonon softening observed in CDFT (see Fig. S7 of SM).

As mentioned earlier, both $2H'$ and $2H''$ phases present additional structural instabilities (see Figs. S8 and S9 of the SM). Concerning the $2H'$ phase, we observe a competition between a 4×4 ($2H'_a$) and $2\sqrt{3} \times 2\sqrt{3}$ ($2H'_b$) periodical distortion. The $2H'_a$ phase is more stable for 0.1 e^-/f.u. $\leq n_e \leq 0.2$ e^-/f.u., while the $2H'_b$ phase is more stable at $n_e = 0.25$ e^-/f.u. At $n_e = 1$ e^-/f.u., the $2H''$ instability (Fig. S5 of the SM, bottom right panel) leads to the $2H''_a$ phase, having a 4×2 periodicity. This further distortion produces an energy gain of 6.6 meV/f.u. with respect to the $2H''$ phase. We underline that the $2H' \rightarrow 2H'_b$ and $2H'' \rightarrow 2H''_a$ represent minor distortions relative to the $2H \rightarrow 2H'$ and $2H \rightarrow 2H''$ distortions, respectively, as demonstrated by the relative energy gain: at $n_e = 0.25$ e^-/f.u. we calculate an energy gain of 107.2 meV/f.u. for the $2H \rightarrow 2H'$ distortion against an energy gain of 3.1 meV/f.u. for the $2H' \rightarrow 2H'_b$ distortion; similarly, at $n_e = 1$ e^-/f.u. we calculate an energy gain of 583.1 meV/f.u. for the $2H \rightarrow 2H''$ distortion against 6.6 meV/f.u. for the $2H'' \rightarrow 2H''_a$ distortion. Whereas, this is not the case for the $2H'_a$ phase: at $n_e = 0.15$ e^-/f.u. we calculate comparable energy gains for the $2H \rightarrow 2H'$ ($\approx$20 meV/f.u.) and the $2H' \rightarrow 2H'_a$ distortion ($\approx$29 meV/f.u.).

Having understood the mechanism leading to CDW formation, we identify possible spectroscopic signatures of the transient phases. In the case of the $2H'$ and $2H''$ structures, we calculate the imaginary part of the dielectric function $\epsilon(\omega)$ allowing both for valence to valence and conduction to conduction optical transitions (absent in the ground state) on top of the valence to conduction ones. In Fig. 3(a), we consider both $2H'$ and $2H''$ phases (solid lines) and their respective distortions (dashed lines) at $n_e =$ 0.25 and 1 e^-/f.u. (see also Fig. S10 of SM). For the

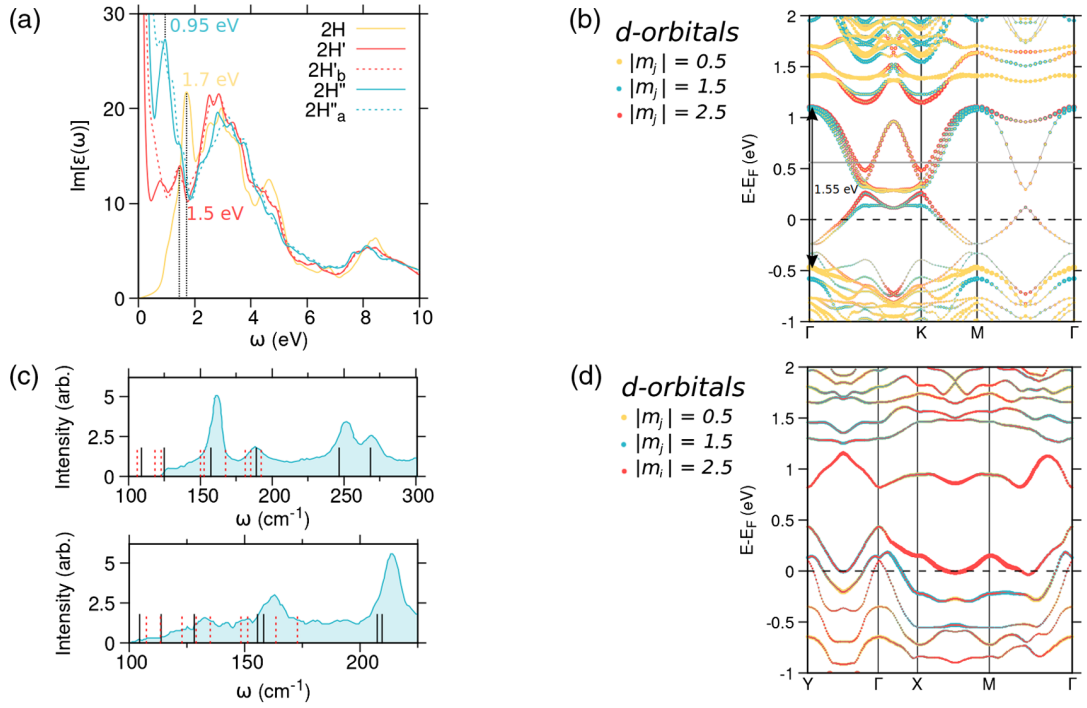

FIG. 3. (a) Imaginary part of $\epsilon(\omega)$ evaluated at $n_e = 0$, 0.25 and 1 e^-/f.u. for 2H-$MoTe_2$ and its distorted phases. (b) Kohn-Sham eigenvalues along the 2H high symmetry BZ path for 2H' $MoTe_2$ at $n_e = 0.25$ e^-/f.u., projected onto atomic d orbitals. Black dashed line (grey line) represents the valence (conduction) quasi-Fermi level. (c) Calculated Raman frequencies (black lines) for 1T'-$MoTe_2$ (top) and WTe_2 (bottom), compared with the experimental Raman spectrum (cyan shaded region) for 1T'-$MoTe_2$ [60] and 1T'-WTe_2 [61]. Red dashed lines represent the Raman frequencies of the 1T'' phase at $n_e = 1$ e^-/f.u. (d) Kohn-Sham eigenvalues along the 1T' high symmetry BZ path for 1T''-WTe_2 at $n_e = 1$ e^-/f.u., projected onto atomic d orbitals.

ground state (i.e., no pumping), our results (see Figs. S11 and S12 of the SM) are in good agreement with previously published *ab initio* results [58,59]. The excited state configuration displays a metallic behavior (Drude peak) both in $MoTe_2$ and WTe_2 [see Fig. 3(a) for $MoTe_2$ and Figs. S11–S14 of the SM for WTe_2 as well as data on reflectance, energy loss and decomposition of $\mathrm{Im}\{\epsilon(\omega)\}$ over optical transitions], which can be recognized from the low-frequency divergence of $\epsilon(\omega)$. This is related to the occurrence of an electron-hole plasma. The main changes in the dielectric function with increasing PC are observed below 2 eV. In particular, the peak observed in the ground state at 1.7 eV, attributed to the valence-conduction optical transition (Fig. S4 of SM, black arrow), is redshifted to 1.5 eV at $n_e = 0.25$ e^-/f.u., as expected when observing the corresponding electronic transition at the $\mathbf{\Gamma}$ point [see Fig. 3(b)]. Furthermore, its intensity is notably reduced. At $n_e = 1$ e^-/f.u. this peak is absent, while a new peak at 0.95 eV not directly related to the valence-conduction contribution appears. Thus, monitoring the evolution of the peak detected at 1.7 eV in the ground state as a function of the PC is equivalent to tracking the band gap closing. The $2H'_a$, $2H'_b$, and $2H''_a$ distortions slightly modify the optical response of the parent structures (see Fig. S10 of SM), causing a small redshift of the 1.5 eV peak for the case of 2H' phase (down to 1.45 eV) and of the 0.95 eV peak (down to 0.89 eV) for the 2H'' phase and changing the Drude peak intensity.

Concerning the 1T' and 1T'' phases, a clear distinction between the two occurs in Raman spectra. The calculated Raman frequencies are shown in Fig. 3(c) for 1T'-$MoTe_2$ and 1T'-WTe_2, and for photoexcited 1T''-$MoTe_2$ and 1T''-WTe_2. Those are compared to the experimental ground state Raman data from Refs. [60,61]. For 1T'-$MoTe_2$, the agreement between theory and experiments is excellent. For the 1T'-WTe_2 phase an overall redshift (≈2%–3% of the value) of the phonon frequencies with respect to the experiment occurs, consistent with previous calculations [62] (see Tab. S4 and the discussion in the SM). We focus on the highest-energy most intense peaks (above 225 cm^{-1} for 1T'-WTe_2 and above 200 cm^{-1} for 1T'-$MoTe_2$), due to phonon modes of A_{1g} and A_{2g} symmetries. The two peaks are well separated in 1T'-$MoTe_2$ and they are strongly overlapping in 1T'-WTe_2, in good agreement with what found in experiments, demonstrating the reliability of our Raman calculations. In the 1T'' phase these two modes are completely absent. Thus, the structural transition is marked by the disappearance of these peaks in both compounds. The calculated Kohn-Sham eigenvalues for 1T''-WTe_2 are depicted in Fig. 3(d): a completely different band structure with respect

to $1T'$-WTe_2 is observed (see also Figs. S17 and S18 of the SM).

In conclusion, by using first principles calculations we have shown that light can be used to unveil hidden CDW order in the transient states of $MoTe_2$ and WTe_2 phases. Pumping on the $2H$ phases leads first to the stabilization of the $2H'_a$ CDW (4×4 spatial periodicity), then to the $2H'_b$ CDW ($2\sqrt{3}\times2\sqrt{3}$ periodicity), and finally to the $2H''_a$ phase (4×2 periodicity). Most important, the $2H'_a$ reconstruction shows an electronic gap that is progressively reduced as a function of fluence, showing a light tunable band gap closing. Thus, inducing a photocarrier population in the $2H$-$MoTe_2$ leads to the following successive transitions: $2H$ (insulating, no CDW) $\rightarrow 2H'_a$ (gapped, 4×4 CDW) $\rightarrow 2H'_b$ (gapless, 2×2 CDW) $\rightarrow 2H''_a$ (gapless 4×2). Given the similar results obtained for $MoTe_2$ and WTe_2, we speculate that similar $2H\rightarrow2H'\rightarrow2H''$ structural transformations occur in other 2D insulating dichalcogenides. We also show that pumping on the $1T'$ at $n_e=1\ e^-/\text{f.u.}$ leads to the transient distorted $1T''$ phase. This new structure is characterized by diamond shaped Mo(W) clusters and a 2×2 periodicity. For each hidden order we identify the spectroscopic fingerprints paving the way to ultrafast measurements of transient states in monolayer dichalcogenides.

Finally, we have shown that the charge ordered phases occurring after laser irradiation are different from those commonly observed in the ground state of metallic transition metal dichalcogenides, such as $NbSe_2$ or $TiSe_2$. Our work demonstrates the presence of new unexpected structural instabilities in this family of compounds.

We acknowledge support from the European Union's Horizon 2020 research and innovation programme Graphene Flagship under Grant Agreement No. 881603. We acknowledge the CINECA award under the ISCRA initiative, for the availability of high performance computing resources and support. We acknowledge PRACE for awarding us access to Joliot-Curie at GENCI@CEA, France (project file No. 2021240020).

*giovanni.marini@iit.it
†m.calandrabuonaura@unitn.it

[1] J. Lloyd-Hughes *et al.*, J. Phys. Condens. Matter **33**, 353001 (2021).
[2] M. Maiuri, M. Garavelli, and G. Cerullo, J. Am. Chem. Soc. **142**, 3 (2020).
[3] F. A. Rasmussen and K. S. Thygesen, J. Phys. Chem. C **119**, 13169 (2015).
[4] X. Qian, J. Liu, L. Fu, and J. Li, Science **346**, 1344 (2014).
[5] Y. Wang, J. Xiao, H. Zhu, Y. Li, Y. Alsaid, K. Y. Fong, Y. Zhou, S. Wang, W. Shi, Y. Wang, A. Zettl, E. J. Reed, and X. Zhang, Nature (London) **550**, 487 (2017).
[6] S. Song, D. H. Keum, S. Cho, D. Perello, Y. Kim, and Y. H. Lee, Nano Lett. **16**, 188 (2016).
[7] S. Cho, S. Kim, J. H. Kim, J. Zhao, J. Seok, D. H. Keum, J. Baik, D.-H. Choe, K. J. Chang, K. Suenaga, S. W. Kim, Y. H. Lee, and H. Yang, Science **349**, 625 (2015).
[8] S. Li, F.-c. Lei, X. Peng, R.-q. Wang, J.-f. Xie, Y.-p. Wu, and D.-s. Li, Inorg. Chem. **59**, 11935 (2020).
[9] M. S. Sokolikova and C. Mattevi, Chem. Soc. Rev. **49**, 3952 (2020).
[10] E. Matsubara, S. Okada, T. Ichitsubo, T. Kawaguchi, A. Hirata, P. F. Guan, K. Tokuda, K. Tanimura, T. Matsunaga, M. W. Chen, and N. Yamada, Phys. Rev. Lett. **117**, 135501 (2016).
[11] C. Ferrante, A. Virga, L. Benfatto, M. Martinati, D. De Fazio, U. Sassi, C. Fasolato, A. K. Ott, P. Postorino, D. Yoon, G. Cerullo, F. Mauri, A. C. Ferrari, and T. Scopigno, Nat. Commun. **9**, 308 (2018).
[12] L. Huang, J. P. Callan, E. N. Glezer, and E. Mazur, Phys. Rev. Lett. **80**, 185 (1998).
[13] C. W. Siders, Science **286**, 1340 (1999).
[14] A. Rousse, C. Rischel, S. Fourmaux, I. Uschmann, S. Sebban, G. Grillon, P. Balcou, E. Förster, J. Geindre, P. Audebert, J. Gauthier, and D. Hulin, Nature (London) **410**, 65 (2001).
[15] C. Paillard, E. Torun, L. Wirtz, J. Íñiguez, and L. Bellaiche, Phys. Rev. Lett. **123**, 087601 (2019).
[16] A. Kogar *et al.*, Nat. Phys. **16**, 159 (2020).
[17] P. Tangney and S. Fahy, Phys. Rev. B **65**, 054302 (2002).
[18] P. Giannozzi *et al.*, J. Phys. Condens. Matter **21**, 395502 (2009).
[19] P. Giannozzi, O. Baseggio, P. Bonfà, D. Brunato, R. Car, I. Carnimeo, C. Cavazzoni, S. de Gironcoli, P. Delugas, F. Ferrari Ruffino, A. Ferretti, N. Marzari, I. Timrov, A. Urru, and S. Baroni, J. Chem. Phys. **152**, 154105 (2020).
[20] F. Schmitt, P. S. Kirchmann, U. Bovensiepen, R. G. Moore, L. Rettig, M. Krenz, J.-H. Chu, N. Ru, L. Perfetti, D. H. Lu, M. Wolf, I. R. Fisher, and Z.-X. Shen, Science **321**, 1649 (2008).
[21] M. Hajlaoui, E. Papalazarou, J. Mauchain, G. Lantz, N. Moisan, D. Boschetto, Z. Jiang, I. Miotkowski, Y. P. Chen, A. Taleb-Ibrahimi, L. Perfetti, and M. Marsi, Nano Lett. **12**, 3532 (2012).
[22] See Supplemental Material at http://link.aps.org/supplemental/10.1103/PhysRevLett.127.257401 for all the simulation details as well as structural and optical characterization of the photoexcited phases.
[23] P. Scherpelz, M. Govoni, I. Hamada, and G. Galli, J. Chem. Theory Comput. **12**, 3523 (2016).
[24] J. P. Perdew, K. Burke, and M. Ernzerhof, Phys. Rev. Lett. **77**, 3865 (1996).
[25] H. J. Monkhorst and J. D. Pack, Phys. Rev. B **13**, 5188 (1976).
[26] C. H. Naylor, W. M. Parkin, Z. Gao, H. Kang, M. Noyan, R. B. Wexler, L. Z. Tan, Y. Kim, C. E. Kehayias, F. Streller, Y. R. Zhou, R. Carpick, Z. Luo, Y. W. Park, A. M. Rappe, M. Drndić, J. M. Kikkawa, and A. T. C. Johnson, 2D Mater. **4**, 021008 (2017).
[27] M. Kan, H. G. Nam, Y. H. Lee, and Q. Sun, Phys. Chem. Chem. Phys. **17**, 14866 (2015).
[28] J. Heyd, G. E. Scuseria, and M. Ernzerhof, J. Chem. Phys. **118**, 8207 (2003).

[29] J. Heyd and G. E. Scuseria, J. Chem. Phys. **121**, 1187 (2004).
[30] A. Splendiani, L. Sun, Y. Zhang, T. Li, J. Kim, C.-Y. Chim, G. Galli, and F. Wang, Nano Lett. **10**, 1271 (2010).
[31] L. Yuan and L. Huang, Nanoscale **7**, 7402 (2015).
[32] A. Chernikov, C. Ruppert, H. M. Hill, A. F. Rigosi, and T. F. Heinz, Nat. Photonics **9**, 466 (2015).
[33] H. Haug and S. W. Koch, *Quantum Theory of the Optical and Electronic Properties of Semiconductors*, 5th ed. (World Scientific, Singapore, 2009), https://www.worldscientific.com/doi/pdf/10.1142/7184.
[34] M. Palummo, M. Bernardi, and J. C. Grossman, Nano Lett. **15**, 2794 (2015).
[35] S. Pan, W. Kong, J. Liu, X. Ge, P. Zereshki, S. Hao, D. He, Y. Wang, and H. Zhao, ACS Appl. Nano Mater. **2**, 459 (2019).
[36] G. Froehlicher, E. Lorchat, and S. Berciaud, Phys. Rev. B **94**, 085429 (2016).
[37] C. Ruppert, O. B. Aslan, and T. F. Heinz, Nano Lett. **14**, 6231 (2014).
[38] H. H. Huang, X. Fan, D. J. Singh, H. Chen, Q. Jiang, and W. T. Zheng, Phys. Chem. Chem. Phys. **18**, 4086 (2016).
[39] D. Alfè, Comput. Phys. Commun. **180**, 2622 (2009).
[40] A. Kokalj, J. Mol. Graphics Modell. **17**, 176 (1999).
[41] K. Momma and F. Izumi, J. Appl. Crystallogr. **44**, 1272 (2011).
[42] X.-B. Li, X. Q. Liu, X. Liu, D. Han, Z. Zhang, X. D. Han, H.-B. Sun, and S. B. Zhang, Phys. Rev. Lett. **107**, 015501 (2011).
[43] D. Erben, A. Steinhoff, M. Lorke, and F. Jahnke, arXiv:2012.07642.
[44] A. Laturia, M. L. Van de Put, and W. G. Vandenberghe, npj 2D Mater. Appl. **2**, 6 (2018).
[45] T. Sohier, M. Calandra, and F. Mauri, Phys. Rev. B **96**, 075448 (2017).
[46] N. Marzari, D. Vanderbilt, A. De Vita, and M. C. Payne, Phys. Rev. Lett. **82**, 3296 (1999).
[47] A. V. Kolobov, P. Fons, and J. Tominaga, Phys. Rev. B **94**, 094114 (2016).
[48] A. Krishnamoorthy, L. Bassman, R. K. Kalia, A. Nakano, F. Shimojo, and P. Vashishta, Nanoscale **10**, 2742 (2018).
[49] Q. Song, H. Wang, X. Xu, X. Pan, Y. Wang, F. Song, X. Wan, and L. Dai, RSC Adv. **6**, 103830 (2016).
[50] J. Lee, F. Ye, Z. Wang, R. Yang, J. Hu, Z. Mao, J. Wei, and P. X.-L. Feng, Nanoscale **8**, 7854 (2016).
[51] Y. Cao, N. Sheremetyeva, L. Liang, H. Yuan, T. Zhong, V. Meunier, and M. Pan, 2D Mater. **4**, 035024 (2017).
[52] Y. Kim, Y. I. Jhon, J. Park, J. H. Kim, S. Lee, and Y. M. Jhon, Nanoscale **8**, 2309 (2016).
[53] W. Yang, Z.-Y. Yuan, Y.-Q. Luo, Y. Yang, F.-W. Zheng, Z.-H. Hu, X.-H. Wang, Y.-A. Liu, and P. Zhang, Phys. Rev. B **99**, 235401 (2019).
[54] M. Calandra, Phys. Rev. B **88**, 245428 (2013).
[55] D. Yang, S. J. Sandoval, W. M. R. Divigalpitiya, J. C. Irwin, and R. F. Frindt, Phys. Rev. B **43**, 12053 (1991).
[56] B. Peng, H. Zhang, W. Chen, B. Hou, Z.-J. Qiu, H. Shao, H. Zhu, B. Monserrat, D. Fu, H. Weng, and C. M. Soukoulis, npj 2D Mater. Appl. **4**, 14 (2020).
[57] C. Si, D. Choe, W. Xie, H. Wang, Z. Sun, J. Bang, and S. Zhang, Nano Lett. **19**, 3612 (2019).
[58] A. Kumar and P. K. Ahluwalia, Physica (Amsterdam) **407B**, 4627 (2012).
[59] In Ref. [58] the intensity of the monolayer dielectric function is incorrectly renormalized due to the presence of the vacuum, an effect that in the paper is incorrectly attributed to the reduced number of bands.
[60] C. H. Naylor, W. M. Parkin, J. Ping, Z. Gao, Y. R. Zhou, Y. Kim, F. Streller, R. W. Carpick, A. M. Rappe, M. Drndić, J. M. Kikkawa, and A. T. C. Johnson, Nano Lett. **16**, 4297 (2016).
[61] Y. C. Jiang, J. Gao, and L. Wang, Sci. Rep. **6**, 19624 (2016).
[62] J. Ma, Y. Chen, Z. Han, and W. Li, 2D Mater. **3**, 045010 (2016).